Research Article

Radar Images of Mars

DUANE O. MUHLEMAN, BRYAN J. BUTLER, ARIE W. GROSSMAN,* MARTIN A. SLADE

Full disk images of Mars have been obtained with the use of the Very Large Array (VLA) to map the radar reflected flux density. The transmitter system was the 70-m antenna of the Deep Space Network at Goldstone, California. The surface of Mars was illuminated with continuous wave radiation at a wavelength of 3.5 cm. The reflected energy was mapped in individual 12-minute snapshots with the VLA in its largest configuration; fringe spacings as small as 67 km were obtained. The images reveal near-surface features including a region in the Tharsis volcano area, over 2000 km in east-west extent, that displayed no echo to the very low level of the radar system noise. The feature, called Stealth, is interpreted as a deposit of dust or ash with a density less than about 0.5 gram per cubic centimeter and free of rocks larger than 1 cm across. The deposit must be several meters thick and may be much deeper. The strongest reflecting geological feature was the south polar ice cap, which was reduced in size to the residual south polar ice cap at the season of observation. The cap image is interpreted as arising from nearly pure CO_2 or H_2O ice with a small amount of martian dust (less than 2 percent by volume) and a depth greater than 2 to 5 m. Only one anomalous reflecting feature was identified outside of the Tharsis region, although the Elysium region was poorly sampled in this experiment and the north pole was not visible from Earth.

FUNDAMENTAL INFORMATION ABOUT THE GEOLOGY OF A planet and its near surface physical structure can be obtained with radar techniques. Radar energy probes into surface deposits of low-density materials to reveal substructures in some cases and the depth of such deposits. Polar ices can, in principle, be sounded on Mars in attempts to understand their structures and composition. The radar properties of part of the equatorial zone on Mars have been measured by a number of investigators (*1*). Mars is much more difficult to observe from Earth in a mapping mode than Venus, Mercury, and the Galilean satellites because the planet's rapid rotation greatly spreads the incident signal in frequency as a result of the Doppler shifts of the local reflecting points (*2*). Most high-resolution investigations have been restricted to a small (~500-km) zone around the instantaneous sub-Earth point on the surface. In this article, we present results of aperture synthesis mapping of Mars using the Very Large Array (VLA) in New Mexico as the imaging instrument to detect continuous wave signals transmitted at 8.5 GHz (3.5 cm) from the Jet Propulsion Laboratory (JPL) 70-m antenna in California (*3*).

The use of the VLA allowed us to map the echoes from the entire visible disk during approximately 12-min intervals. The radar system was also recently used to image Titan (*4*). The Mars observations are very different from those on Titan because for Mars the VLA A-array (36-km maximum spacings) was used and Mars subtended a large angle on the sky. As a result, the pixel resolution was 80 km on the sub-Earth point. The echoes were mapped in snapshots in the spectral line mode of the VLA with the use of 63 frequency channels (3252-Hz bandwidth), 9 of which contained echo energy attributed to the total Doppler rotational spreading of ~25 kHz. All of the channels contained the thermal emission from Mars. The observations were made in southern hemisphere late spring, l_s was 295° the sub-Earth longitude, and the sub-Earth latitude was −24° (*5*). An image was made of the entire visible hemisphere for each snapshot for the 8-hour view period (*6*); in all, 38 images were obtained that cover 80% of the planet's surface. Six of these images at approximately hourly intervals are shown in Fig. 1.

The transmitted signal to Mars was right circularly polarized (RCP), and both RCP and left circularly polarized (LCP) echoes were received and mapped. As expected, the LCP echoes were dominated by the so-called specular (or phase-coherent) reflections at near-normal incidence in the first Fresnel zone (350 m) on the sub-Earth point (7). The RCP or depolarized echoes were free of this specular spike and revealed the surface and subsurface structure over most of the planet's surface. We will use OS for the opposite sense of received versus transmitted polarization and SS for the same sense for depolarized echoes. Although most structures can be seen in the OS maps as diffuse reflections when they were away from the sub-Earth region, these images are affected by grating lobes caused by the specular spike and are not discussed (*8*).

The reflection of even a plane wave of any polarization from a surface or medium that can only be defined with statistical boundary conditions is a highly complex and poorly understood phenomenon. Radar images of such reflections only contain the power from each pixel region and lack phase, time delay, or other information on the depth to a reflecting layer. There is some certainty that the echoes in the OS mode in the specular spike were created at the true surface layer, but the diffuse component and all of the SS energy must come from multiple reflections at the surface and in the layers below the surface (7). It is believed that subsurface reflections are most important for producing the depolarized reflections, but a small component of multiple reflections from the surface is not ruled out.

Observations. The images (Fig. 1) show that almost all of the SS echo energy comes from regions in the Tharsis volcano area except for the strongest return, which comes from the residual south polar ice cap (RSPIC). The RSPIC lies a few degrees from the south pole.

D. O. Muhleman, B. J. Butler, and A. W. Grossman are with the Division of Geological and Planetary Sciences, California Institute of Technology, Pasadena, CA 91125. M. A. Slade is with the Jet Propulsion Laboratory, California Institute of Technology, 4800 Oak Grove Drive, Pasadena, CA 91109.

*Present address: Department of Physics and Astronomy, University of Maryland, College Park, MD.

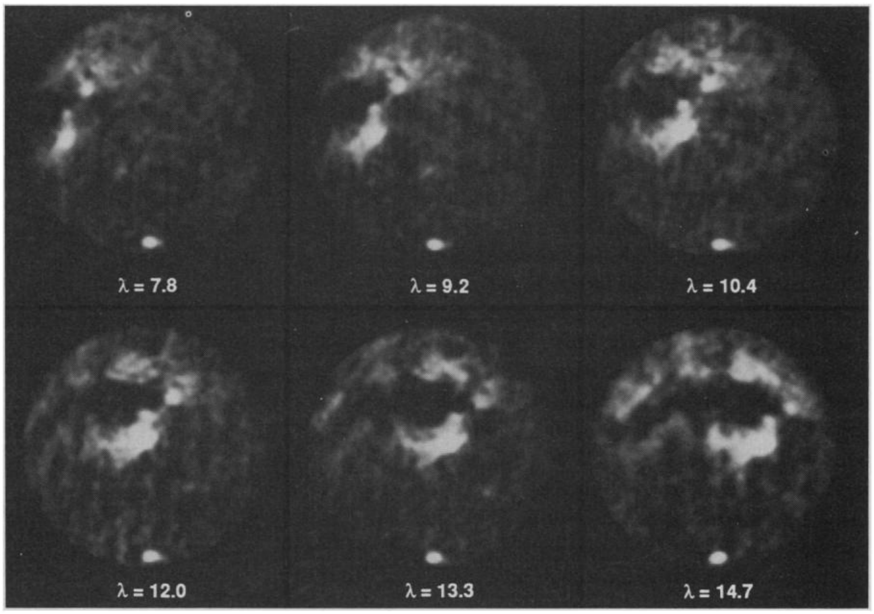

Fig. 1. Six snapshot images made in the depolarized or SS mode. The images are labeled with the Mars longitude of the sub-Earth point and are roughly 1 hour or 15° in longitude apart. Each image is a 12-min exposure.

All of the major radar features identified on the martian surface that were consistently stronger than their environs are listed in Table 1. The remainder of the observed surface did not display echoes greater than 0.25 millijansky per beam [1 jansky (Jy) = 10^{-26} W m^{-2} Hz^{-1}]. We have named each feature, which is usually the standard name of the nearby visual feature. All of the features with strong radar echoes except the south feature are in the Tharsis volcanic region (*9*). It is important to note that we did not adequately observe the Elysium complex or the Hellas basin.

A radio telescope such as the VLA measures the flux density of point sources, usually expressed in janskys, or the source surface brightness in jansky per beam for spatially resolved sources where "beam" means the solid angle of the synthesized beam. The pixels in the images are 0.20 arc sec and the synthesized beam diameter is 0.5 arc sec. The second column in Table 1 lists the peak radar brightness in the feature and its root-mean-square (rms) value obtained from averaging the brightest pixel of the feature over the ensemble of snapshot maps. The last column lists the extent of the feature or the rms wander of the brightest pixel over the ensemble average of the feature. A north-south extent of about 80 km means that the wander of the bright pixel was about one pixel. The east-west resolution is apparently larger as a result of the 12-min smear in each image in addition to the real extent of the feature. The data of Table 1 suggest that only the RSPIC, South Tharsis, and Olympus Mons features were resolved by the beam. "Stealth" (Table 1) is a special case where no return was detected over a huge region on the equator. It extends from the west flank of the Tharsis volcanoes into Mesogaea, far to the west. The last line of the table shows the mean depolarized response of Mars averaged over the visible disk; the average is calculated for an observed falloff with incidence angle proportional to cosine of the angle. The data show that the features (except Stealth) are significantly stronger than all surrounding terrain.

The expected return from a surface element can be computed from a knowledge of the radar parameters (*4*) and the ephemeris of Mars (*5*). If the power transmitted at wavelength λ is P_t, the echo power in a synthesized beam solid angle is (in watts per beam)

$$P_r = \frac{P_t A_t A_r \Omega_b}{4\pi\lambda^2 D^2}\eta(\theta) \qquad (1)$$

where η is the surface reflectivity, which is generally a function of the incidence angle θ, Ω_b is the solid angle of the beam, A_t and A_r are the effective areas of the transmitting and receiving antennas, and D is the distance to Mars. The flux density in a beam solid angle or the radar brightness is P_r divided by A_r and the effective bandwidth of the receiver, in this case the spectral channel width. Putting in the radar and ephemeris parameters, we find that the radar brightness is

$$F_r = 1.89\eta(\theta) \text{ Jy/beam} \qquad (2)$$

which can be used to compare the measured values in Table 1. The agreement of Eq. 2 with $\eta = 1.0$ and the mean reflectivity of RSPIC is remarkable; the cap is essentially a perfect radar reflector. A surface that scatters uniformly into 4π stercadians without absorption has this property. The reflectivity of the south cap remained nearly constant over the experiment, as is consistent with the constant incidence angle of the pole of 66.2°. Although the OS images of the RSPIC are strongly corrupted by grating lobes, we can say with confidence that the SS reflectivity is greater than the OS reflectivity; this conclusion is consistent with other radar measurements of cold ice on Europa, Ganymede, and Callisto (*10*). The south polar ice cap waxes and wanes throughout the martian seasons but never vanishes, and a residual cap persists throughout the southern summer (*11*). The RSPIC is thought to be composed primarily of CO_2 because the measured temperature apparently remains at ~148 K, that is, below the CO_2 frost temperature, and the cap frost remains in equilibrium with the CO_2 atmosphere (*12*). The cap is, of course, sufficiently cold to hold H_2O and it may also be a major reservoir of water.

Residual south polar ice cap. Our measurements of the RSPIC indicates that it acts like a deep diffuse scatterer at the radar wavelength. Such a structure exhibits multiple scattering with a strong tendency toward backscattering. Chandrasekhar (*13*) has obtained the exact solution of the radiative transfer problem for the reflection from a plane parallel isotropic scattering medium that is infinitely deep with randomly polarized radiation incident from above. Our radar illumination was RCP, and the radiation reflected from the top of the structure, if the scattering was strictly isotropic, may have contained slightly more LCP than RCP, proportional to the amount of the radiation that is single-scattered from the medium (*7, 13*). This amount is small for highly reflecting multiple scatterers considered here. However, Chandrasekhar's result would apparently be approximately correct for the depolarized reflected flux after a factor of 1/2 is introduced to account for our measurement of a single reflected polarization sensed by the VLA receivers. The resulting expression for the brightness is (in jansky's per beam)

$$F_r = \frac{\omega P_t A_t \Omega_b H(\mu)^2}{16\pi\lambda^2 D^2 BW} \qquad (3)$$

where $H(\mu)$ are the H functions tabulated in (*13*), $\mu = \cos\theta$, and ω is the single scattering albedo of the medium, that is, the ratio of the scattering to the extinction coefficients. Curves from Eq. 3 for four values of ω are shown in Fig. 2. We also show our measurement of the peak brightness of the RSPIC (Table 1) where we have augmented the rms error by our estimate of the total radar system error (*4*). This work suggests that the cap is indeed a deep, nearly isotropic scattering medium and that $\omega \sim 1.0$, corresponding to a conservative scattering medium. Pure ices of CO_2 and H_2O at these

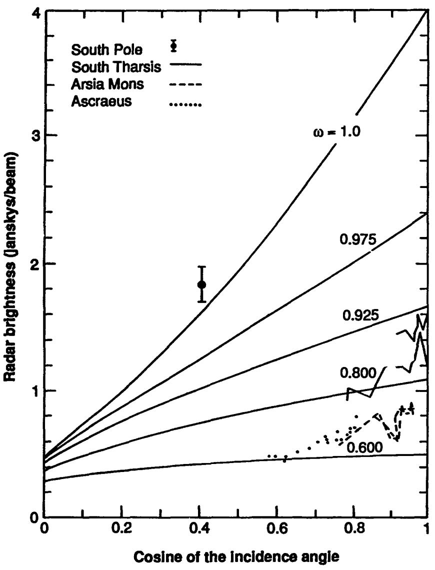

Fig. 2. Radar backscatter brightness as a function of incidence angle. The singular data point is the average brightness of the south polar ice feature which had a fixed incidence angle. Brightness curves for the Ascraeus Mons, Arsia Mons, and the South Tharsis features, both pre- and post-meridian, are indicated. The smooth lines show the expected response from the multiple scattering theory, Eq. 3, for several values of ω.

temperatures are highly transparent at microwave frequencies (*14*), and a formal interpretation of this result is that the ice is clean, that is, relatively free of martian soil. We can make a crude estimate of how clean the ice is by comparing the single scattering albedo for an ice sphere of radius, say, our wavelength, to that of an ice sphere containing a small amount of martian soil. The details of the soil distribution in an ice particle are not important, only the integrated effect. Assuming that the parent source of the soil is a typical basaltic rock (*15*) with density 3 g cm^{-3} and complex dielectric constant $(7.0 - i\,0.42)$, we find that ω of an ice sphere is 0.925 if it contains 1.7 percent soil by volume and 0.889 for 3.3 percent soil. The albedo for the pure ice sphere is 0.9999. However, we can only put a crude limit of less than 5 percent soil from our data. It can be seen from the curves of Fig. 2 that even these traces of soil would significantly depress the reflectivity. Paige and Ingersoll (*12*) have investigated the seasonal variations of the visible albedo of the ice caps which may, or may not be related to the radar reflectivity.

We can gain some understanding as to the depth of the ice cap by assuming that the above interpretation is exactly correct. We have made a crude estimate of the lower limit on the cap thickness such that it would act like an infinitely deep, conservative, isotropic scatterer. We used Monte Carlo computer trials to simulate the problem and to bound the depth. The photons were normally incident on a conservative scattering medium and were then isotropically scattered from centers that were a mean free path, L, apart. All incident photons in the model calculation ultimately came back out of the medium for conservative scattering, and the deepest depth of penetration of each photon was counted (Fig. 3A). The experiment was repeated several times with similar results. Scatterers on the surface were excluded because they would overwhelmingly contribute as single scatters and would not be seen in the depolarized echo. Although the scale depth of this phenomenon is just 2.8 scattering lengths, a much better estimate of the minimum depth for the observed reflectivity measurement is the depth for which ~95 percent of the photons were returned without hitting the substrate (Fig. 3B). The depth turns out to be $21L$ from the integration of the histogram (Fig. 3). Obtaining an accurate estimate of L is difficult, however. The scattering phenomenon is caused by the encounter of the radar wave with a jump in impedance or dielectric constant. The jumps associated with the martian ice cap are probably caused by one of the following structures: (i) open cracks or crevices in the ice sheet, (ii) chunks of denser ice in a frost matrix, or (iii) voids in the frost or ice matrix. Apparently, these heterogeneities do not anneal in the martian ice cap. We have crudely modeled the structure with spherical scatters of radius R with separations $L > 2R$. Defining the volume packing factor of the medium, P, as the ratio of the volume of the scatterers in a unit cube to the volume of the cube, we get

$$L \approx R(4\pi/3P)^{1/3} \tag{4}$$

A scattering element smaller than one wavelength will not be an efficient scatterer, and scatterers much larger than one wavelength will tend to create an anisotropic scattering medium. Thus, we estimate that $R \approx \lambda = 0.035$ m. Our admittedly crude estimates of the thickness of the RSPIC of $\approx 20\ L$ are shown in Table 2 as a function of packing factor P.

Thus, our best estimate is that the ice sheet is deeper than a few meters but could be as shallow as 1 m if the surface is a pile of ice spheroids 3.5 cm across. The ice could be much thicker than this, a supposition that can be supported with geological arguments. Current theoretical models (*12*) predict that the thickness of the annual variations of the south polar CO_2 ice sheet is also about 1 m, but this layer would have sublimated away by the time of our observations. The observations do not discriminate between CO_2 and H_2O ice particles, both of which would exhibit $\omega \approx 1.0$.

The Stealth region. Perhaps our biggest surprise from the experiment was the discovery of the feature we call Stealth, which lies along the equator and extends from the west flank of Arsia Mons westward for about 2000 km. It can be seen in all the images in Fig. 1, and its full extent is best seen in the image at central meridian longitude 147°. The feature appears in each depolarized snapshot map as an amorphous region with a flux consistent with the noise on

Table 1. Major depolarized features.

Name*	Brightness† (Jy per beam)	Longitude (degrees)	Latitude (degrees)	Extent (km)‡ (north-south by east-west)
RSPIC	1.83 ± 0.04	53.2	−87.4	80 by 90
South Tharsis	1.31 ± 0.05	121.9	−21.0	85 by 240
Pavonis Mons	0.88 ± 0.02	107.4	0.6	85 by 100
Arsia Mons	0.77 ± 0.02	119.5	−9.1	80 by 100
Olympus Mons 1	0.70 ± 0.02	124.3	16.5	300 by 600
Olympus Mons 2	0.47 ± 0.02	156.5	14.9	185 by 260
Ascraeus Mons	0.64 ± 0.02	102.8	11.0	100 by 120
South Feature	0.36 ± 0.05	93.4	−40.9	70 by 140
Stealth	0.0 ± 0.02	125 to 168	0	500 by 2300
Average surface§	$\sim(0.15 \pm 0.02)\cos\theta_I$			

*The name is either taken from a nearby feature or invented here. †The brightness is the average of the brightest pixel from each snapshot and the rms value about this mean. The longitude and latitude value is the mean position of the brightest pixel averaged over the snapshots. ‡The extent is the rms wander of the surface position of the brightest pixel from the snapshots. It tends to be smaller than the region of half-brightness relative to the peak. For example, RSPIC is roughly 300 km in diameter but the brightest point is smaller. §θ_I is the angle of incidence of the radar beam.

Table 2. Estimates of the minimum thickness of the RSPIC.

Packing factor	L (meters) (m)	Minimum thickness (m)
0.01	0.26	5.2
0.03	0.18	3.6
0.10	0.12	2.4
0.30	0.08	1.6

each pixel, which is about a factor of 10 less than the average for the full disk, that is, less than about 0.02 Jy per beam. This value corresponds to a reflectivity of less than 1 percent on the basis of Eq. 2. Thus, this region is identical to the average region in the maps off the Mars disk (not shown in Fig. 1). Opposite sense echoes are also not recorded from Stealth, but that can be partially understood because it was never viewed at an incidence angle of less than 20° from the normal (*16*). However, all the other features listed in Table 1 can be found in the OS maps, apparently because they are all detectable diffuse reflectors. Stealth is not a detectable diffuse reflector even in the OS or polarized mode of observing. Because of the amorphous nature of the observed feature caused by noise without true signal, we adopted the criterion that a pixel region is in Stealth if the signal was at or below the noise for three consecutive snapshots. Our best estimate of the Stealth feature is shown by the two enclosed contours on the map in Fig. 4. The west part (left in Figs. 1 and 4) is mostly confined to the Medusae Fossae feature near 3°S160°W in a region called Mesogaea. The eastern region is separated by the cratered highlands containing Magala Vallis and extends partly up the flank of the Arsia Mons volcano within about 350 km of the caldera. The east feature slopes from an altitude of about 8 km westward to 2 km as Medusae Fossae is approached. We estimate that our accuracy in defining Stealth is about ±50 km in the boundaries and somewhat better at the east edge near Arsia. No consideration of the geological features known from photographic images was made to avoid bias. It is likely that small regions within our boundaries are nominal reflectors that were overlooked by our procedures.

The geology of parts of this region has been studied by Schultz and Lutz, and several groups (*17*) who reported that the region appears to contain a very thick deposit (on the order of kilometers); formed from a loosely packed collection of material; the surface has undergone extensive wind erosion. The important question is what

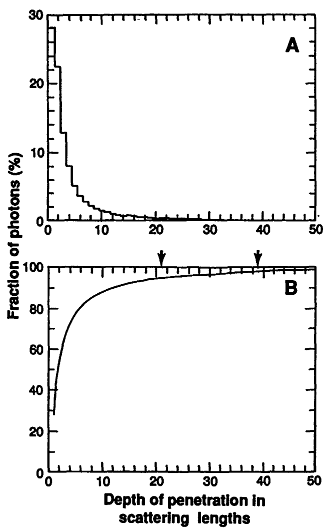

Fig. 3. Monte Carlo simulations of the depths of penetration of photons into a semi-infinite half space of a conservative scattering medium with a fixed separation distance between scatters. (**A**) The fractions of the photons penetrating to a given depth before ejection from the top, and (**B**) the accumulated fraction of photons ejected from the top, both in units of the number of scattering lengths. The arrows show the penetration depths for 95 and 99 percent of the incident photons.

is the deposit? While we are certain that the OS and SS reflectivities are not exactly zero, we are equally sure that the region is a very poor reflector of radio waves. No other features that meet our criterion have been found on Mars, and, as far as we know, no such regions have been found on the moon or Venus. It has been shown, however, that a region of deep volcanic ash on Kilauea in Hawaii has similar characteristics in radar sounding (*18*). The Stealth characteristics could be explained with two extreme end-member models: (i) an infinitely deep half-space whose impedance is matched to free space, that is, of unity dielectric constant, totally free of volume scatterers to considerable depth, or (ii) a metal surface slightly tilted off the normal, or the equivalent perfectly smooth surface such that the incident wave does not penetrate, and subsurface volume scatterers are not encountered. A perfectly smooth surface made of ordinary or dense martian materials can be ruled out because the region has also been found to exhibit near-unity microwave emissivity (*17*). Most of the martian surface exhibits a microwave emissivity consistent with a soil density of about 1 g cm^{-3} plus a nominal rock fraction.

The first model is the closest to being physically sensible, and we pursue that idea. The surface layer must have a low dielectric constant, have significant absorption to render the sublayer (bedrock or nominal consolidated soil) invisible, and be free of subsurface scatterers, unlike the ice cap or other radar features. The region exhibits very low thermal inertias (*19*); this characteristic strongly suggests that the surface layer is an underdense, insulating material (and not, of course, metallic). The strong Arsia Mons feature is also a region of very low thermal inertia, but unlike Stealth, it apparently possesses volume scatterers. We have computed the normal-incidence reflectivity of a homogeneous layer of depth D, described by its complex dielectric constant, over a dielectric half space with properties of the mean martian surface. The results of this calculation are shown in Table 3 where the depths in the last column are layer thicknesses for which the reflectivities are within 10 percent of the value for an infinitely thick layer of the material (*20*). We used the listed values of the dielectric constants for geological materials expected to be found on Mars in powder form (*15*). The values were scaled from laboratory measurements of basalt powders with a density of 1 g cm^{-3} with the use of well-established scaling laws related to the Lorentz-Lorenz relation (*15*). The listings in parentheses have one-half of the imaginary part of the dielectric constant above it, corresponding to less mafic materials, that is, with less elemental iron. The radar data suggest that a layer with a density less than about 0.5 g cm^{-3}, completely free of volume scatterers (for example, rocks), and at least 1 to 3 m deep would account for the observations. Materials with densities greater than this would not exhibit the observed properties. In any case, the enormous size of the underdense deposit and lack of any radar scatters such as rocks remains a great challenge to explain.

The location of Stealth adjacent to the Tharsis region, combined with the properties described above, suggests that Stealth is a massive eolian deposit associated with the Tharsis volcanoes. Lee *et al.* (*21*) interpreted wind streaks near Tharsis seen in Viking images as evidence for downslope winds from east to west off of the volcanoes, Arsia Mons in particular. They pointed out that the low thermal inertia of the region implies that diurnal temperature variations are large and could drive the winds. Our interpretation of the formation of Stealth then is that materials from pyroclastic eruptions of the Tharsis volcanoes have been blown westward into the Stealth region, where they have collected to form an underdense unconsolidated blanket of material. Similar arguments can be found in the literature (*21*). The pyroclastic material itself could be ash flow or ash fall tuff, a hypothesis by Scott and Tanaka (*22*), or very vesicular pumice (for example, reticulite). If, instead, the structure

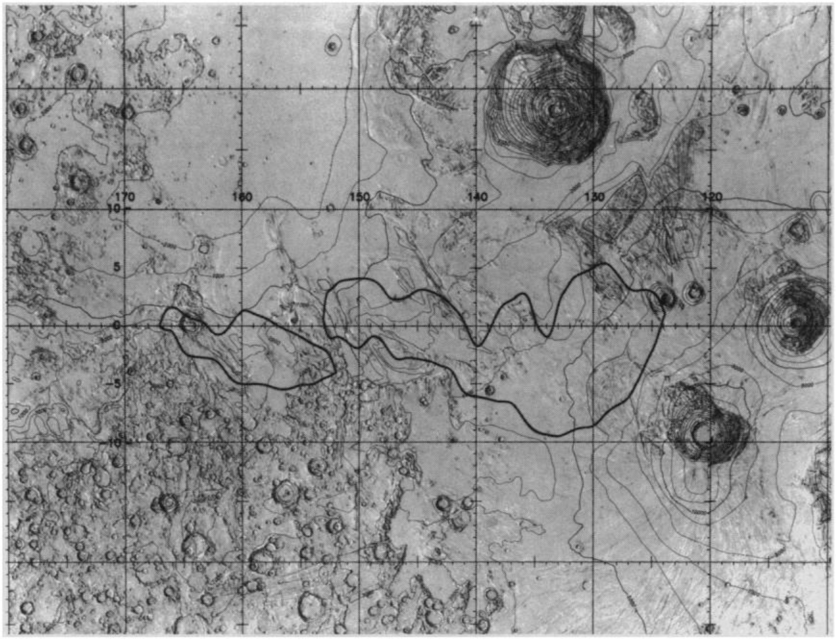

Fig. 4. Contour outline of the Stealth region on the USGS MAP I-2030. The contour is accurate to about 100 km over most of the feature with considerably more uncertainty in the northwest.

was created by a low-viscosity lava flow, the surface would have to be remarkably smooth on the scale of our wavelength (highly unlikely) or be underdense or frothy (also unlikely). In any case, the material must have sufficient strength to support several meters of weight over eons yet must still be underdense; this constraint argues against the source being dust settling out of dust storms.

Other anomolous features. Four of the remaining features are directly associated with the volcanoes, and all lie at high altitudes. It is reasonable to expect that they are characterized by extreme roughness, ash deposits, and strong volume scattering. High-resolution Viking images show that the South Tharsis feature is a complex collection of fairly young, relatively thin, overlapping lava flows (*22*). Such flows at the surface or buried in stealth-like materials would be strong diffuse reflectors. For discussion, we will assume, simplistically, that they may be explained in terms of volume scattering. The reflectivities for the brightest pixel as a function of incidence angle in South Tharsis, Arsia Mons, and Ascraeus Mons are shown in Fig. 2. The features are essentially unresolved by our beam and they should show consistent reflectivity curves for premeridian and postmeridian observations. The behavior of the brightest pixel for South Tharsis, which is resolved by our beam, is not so consistent. The reflectivity curve for Pavonis Mons is not shown because it is nearly identical to the curve for Arsia Mons. The curves are reasonably consistent with the simple isotropic, multiple-scattering theory, and the associated values of ω roughly agree with values computed for martian rocks with sizes equal to the wavelength, with densities of about 2 g cm^{-3}, and buried in a matrix of underdense martian soil. However, a large set of combinations of rock densities and sizes can be found that fit the observations. Obviously, this is not the only possible interpretation of the data and further work is needed (*8*).

Conclusions. Most of the reflected energy in the depolarized radar mode comes from subsurface reflectors. The most remarkable feature found on Mars is Stealth, which fails to return any energy to a very low value of measured reflectivity. A reasonable model of the structure is a deposit of martian ash with a density less than about 0.5 g cm^{-3} and a depth greater than about 2 m, perhaps much less dense and much deeper. Thermal inertia and microwave emissivity measurements reveal that Mars is covered with materials having densities near unity and containing abundant rocks. The location of Stealth suggests that the deposit was formed by strong downslope winds off the Tharsis volcanoes and possibly Olympus Mons that scoured pumice-like materials from the flanks and caldera of the volcanoes. Because these measurements were done with a short wavelength (3.5 cm), it is likely that the deposit is significantly deeper than 2 m and that only its upper part has been sampled.

Equally remarkable is the reflection measured from the planet's south pole seen at an elevation angle of about 24°. Essentially all of the energy is coming from the RSPIC, which acts like a radar-white, diffuse scatterer. If the ice layer was homogeneous and smooth, an echo at the observed incidence angle would not have been detectable, and the only way we can account for the very strong reflections is to invoke conservative, multiple scattering in an inhomogeneous ice structure that includes fractures, lumps, or voids. It is not clear why such a structure would not anneal to a homogeneous mass in a short time. The deposit must be at least a few meters deep.

Finally, there is a region of Mars that has barely been observed as yet—the entire subsurface. Although thermal inertia maps made with infrared instruments on the Viking Orbiter (and those on other missions) yielded significant information about the upper few centimeters, nearly everything below remains unexplored. We have presented maps and interpretations of depolarized radar reflectivities made at a short wavelength, 3.5 cm, which apparently sounded the subsurface to a few meters over several singular features. It is not clear for the remainder of the planet sampled whether the subsurface was probed or the monotonous reflection phenomena were dominated by surface reflections, that is, the impedance jump at the atmosphere-surface interface.

The study of Mars would greatly benefit from an aggressive radar astronomy program at longer wavelengths. The program could be carried out with the VLA if the antennas were outfitted with 13-cm wavelength receivers, but the ultimate scientific investigation would require placing in near orbit around Mars a radar system with even longer wavelengths and full polarization capability. Such an instrument must include the capability to map the thermal emission from the surface at the same wavelength to greatly assist in understanding the relative components of multiple scattering effects and the more interesting phenomena associated with regolith depths and physical

Table 3. Depth of a Lossy dielectric sheet over a dielectric half-space that makes the conductor effectively invisible.

Density* (g cm^{-3})	Dielectric constant†	Reflectivity infinite layer (%)	Minimum depth (m)
0.1	1.077 − i0.00086	0.03	3.2
(0.1)	(1.077 − i0.00043)	(0.03)	(5.8)
0.2	1.16 − i0.0019	0.14	1.3
0.4	1.33 − i0.0043	0.51	0.65
(0.4)	(1.33 − i0.00215)	(0.51)	(1.25)
0.6	1.53 − i0.0073	1.12	0.45
0.8	1.75 − i0.0112	1.93	0.25
1.0	2.00 − i0.0160	2.95	<0.2

*The listings in parentheses have one-half the imaginary part of the dielectric constant above it, corresponding to less mafic materials, that is, less elemental iron. †Values for basaltic powders, packed with bulk densities given in column 1.

parameters such as densities and particle or rock-fragment sizes. An impressive geological and geophysical reconnaissance of Mars would be made similar to that by Magellan at Venus but with subsurface sounding.

REFERENCES AND NOTES

1. The first reported variations of radar cross section with longitude for Mars were by R. M. Goldstein and W. F. Gillmore [*Science* **141**, 1171 (1963)] at 13-cm wavelengths and Kotel'nokov *et al.* [*Dokl. Akad. Nauk.* **151**, 811 (1963)] at 39 cm. Definitive repeatable variations were obtained at 70-cm wavelengths from Arecibo Observatory in 1965 [R. B. Dyce, G. H. Pettengill, A. D. Sanchez, *Astron. J.* 72, 771 (1965)]. Measurement of topographic variations at 3.8 cm from Haystack Observatory quickly followed during the oppositions of 1967, 1969, and 1971 [for example, G. H. Pettengill, A. E. E. Rogers, I. I. Shapiro, *Science* **174**, 1321 (1971)]. A large set of data at 13 cm, including topography, large-scale slopes, rms surface tilts, and reflectivity, was collected during the 1971 and 1973 oppositions from Goldstone [G. S. Downs, P. E. Reichley, R. R. Green, *Icarus* **26**, 273 (1975)].
2. Delay Doppler mapping is performed by transmission of a coherent series of pulses, followed by analysis of the echoes in both range and frequency. Because the target bodies are typically rotating and nearly spherical in shape, an inversion of the maps from the delay Doppler shift regime to a latitude-longitude coordinate system can be made, albeit usually with ambiguities on either side of the Doppler "equator." Mars rotates rapidly compared to Mercury and Venus, and therefore has a large Doppler bandwidth, *BW*. The delay Doppler technique in its simplest form requires that only one delay pulse be sampling the delay depth τ_0 of the planet. A large Doppler bandwidth, however, requires a high-pulse repetition rate to avoid aliasing in frequency. Simple delay Doppler mapping thus requires that $BW(\tau_0)$ be less than 1. This condition is violated by all the terrestrial planets at usual observing wavelengths (they are "overspread"). However, the strong specular dependence of the scattering law of the surfaces of Venus and Mercury often allows the aliased power to be ignored within the limited number of range samples permitted by current hardware constraints. The surface of Mars is very heterogeneous. This heterogeneity, combined with the rapid rotation rate, sometimes causes the aliased power to be significant within the accessible spherical cap. Conclusions about the true reflectivity of the surface of Mars with the use of delay Doppler mapping are thus fraught with possible error. At the same time, continuous wave (CW) observations have been performed on Mars, primarily at Arecibo. CW data contains information about the entire visible disk of the planet, whereas delay Doppler ranging is limited to a small spherical cap about the subradar point. These observations have revealed information about the surface properties of Mars unobtainable from ranging alone [for example, J. K. Harmon and S. J. Ostro, *Icarus* **62**, 110 (1985)].
3. The 70-m antenna at Goldstone, CA, is part of the NASA Deep Space Network operated by the Jet Propulsion Laboratory. The Very Large Array near Soccoro, NM, was built and operated by the National Radio Astronomy Observatory (NRAO).
4. The radar transmitter consisted of the Goldstone 70-m antenna and a 360,000 (±5 percent)-watt, 8.495-GHz CW transmitter. The value of the effective area of the antenna is 2616 (±3 percent) m^2 at an elevation angle of 29°. The receiving instrument was the NRAO VLA consisting of 27 antennas (diameter 25 m) with an effective collecting area of 7952 (±5 percent) m^2.
5. Mars was observed for 12 hours on 22 October 1988 when its geocentric distance was 0.46 AU and the martian latitude of the subearth point was −24°. The season on Mars was early summer in the southern hemisphere with $L_s = 295°$.
6. The antennas at the VLA are in a Y configuration with one arm ~5° off north. For this experiment the antennas were in the A array where the maximum antenna spacings between arm ends was 36 km. The minimum fringe spacing was 0.2 arc sec or 67 km on Mars. Because images were made during each 12-min interval, the rotation of the baselines projected on Mars was negligible. The amplitudes and phases of the instrument were calibrated between each snap shot by observation of the point source 0006–063, whose flux density was measured to be 1.61 Jy, on the basis of the known flux density of 3C48. The phases were then self-calibrated with the method of phase closure on the specular radar spike from the martian sub-Earth point. The beam resulting from the known antenna configuration was deconvolved from each channel map containing returned energy from Mars for each of the snapshots with the use of the CLEAN algorithm. The resulting channel maps were finally summed to construct the final image for each snapshot.
7. The backscatter reflection from a perfectly smooth dielectric sphere illuminated with circular polarization will arise from the first Fresnel zone and will be completely circularly polarized in the opposite sense. See, for example, J. A. Stratton, *Electromagnetic Theory* (McGraw-Hill, New York, 1941), chap. 9. An actual planetary surface with topography presents numerous convex surfaces with radii of curvature similar to the planetary radius that intermittently contribute phase-coherent echoes and as such, are primarily polarized in the OS of the incident waveform. Even the diffuse reflections from planetary surfaces usually have more flux in the OS mode than in the SS mode and it is reasonable to assume that the differences are due to single scattering off of structures with curvature radii near the wavelength. Apparently, most of the diffuse echo energy in both polarizations comes from multiple scattering at and beneath the surface.
8. B. Butler, D. Muhleman, A. Grossman, M. Slade, in preparation.
9. Much of the surface of Mars was sensed in both polarizations with the use of the CW Doppler spectrum technique discussed by J. K. Harmon and S. J. Ostro [*Icarus* **62**, 110 (1985)] and J. K. Harmon, M. Slade, J. Alexander, in preparation.
10. Radar echoes from Ganymede were obtained first by R. M. Goldstein and R. R. Green [*Science* **207**, 179 (1980)]; see also D. Campbell *et al.*, *Icarus* **34**, 254 (1978) and S. Ostro, in *Satellites of Jupiter*, D. Morrison, Ed. (Univ. of Arizona Press, Tucson, AZ, 1982), p. 213. When illuminated with a circular polarized wave, Europa, Ganymede, and Callisto exhibit stronger echo in the SS of polarization than in the OS. An important explanation of this phenomena in terms of "coherent multiple backscatter" has been presented by B. Hapke [*Icarus* **88**, 407 (1990)]. We believe that this phenomenon is important in the radar scattering from the martian south pole.
11. M. H. Carr, *The Surface of Mars* (Yale Univ. Press, New Haven, 1981), and references therein.
12. The thermal balance on the surface of Mars was originally discussed by R. B. Leighton and B. C. Murray [*Science* **153**, 136 (1966)]; the observational evidence and theoretical implications have been presented by D. A. Paige and A. P. Ingersoll [*ibid.* **228**, 1160 (1985)] and D. A. Paige, K. E. Herkenhoff, and B. C. Murray [*J. Geophys. Res.* **95**, 1319 (1990)].
13. S. Chandrasekhar, *Radiative Transfer* (Dover, New York, 1950), chap. 3. The theory of isotropic scattering was developed for natural light scattered in a medium where the separations between centers were large compared to the wavelength and each center scattered isotropically; these conditions suggest that particles are small compared to the wavelength. B. Hapke [*J. Geophys. Res.* **86**, 3039 (1981)] has demonstrated experimentally that these ideas are a good approximation for scattering from a loosely consolidated surface with scatterers large compared to the wavelength. B. Hapke [*Icarus* **88**, 407 (1990)] has applied the concept of "coherent backscatter" to the radar reflection problem.
14. O. Mishima, D. D. Klug, E. Whalley, *J. Chem. Phys.* **78**, 6399 (1983).
15. M. J. Campbell and J. Ulrichs, *J. Geophys. Res.* **74**, 5867 (1969).
16. The most reliable way to probe the Stealth region would be at normal incidence. However, the sub-Earth point at Mars during times of close approaches has never crossed the Stealth region since development of planetary radar. Our measurements show that even in OS polarization the diffuse echo is down from that of the environs by nearly a factor of 100. Recently, measurements by R. Jurgens and M. Slade (unpublished data) passed over the southern edge of Stealth and showed a decrease in OS, normal incidence reflectivity of a factor of 100. R. A. Simpson, G. L. Tyler, and B. J. Lipa [*Icarus* **32**, 147 (1977)] discuss the significance of the highly variable martian radar reflectivity.
17. The presence of a stealth-like region but not its significance was suggested in the data from D. Rudy, D. O. Muhleman, and G. L. Berge (in preparation). The 2- and 6-cm brightness temperatures of Mars were mapped in February 1985 at the VLA in full day synthesis images (Mars longitudes of 33° to 190°) during a time when the full longitudinal extent of Stealth was smeared through the maps (plus other terrain). The ratio of the measured brightness temperature to the thermal model temperature in the latitude band from 0° to 5°N corresponds to an effective surface dielectric constant of 1.4 ± 0.4, which the investigators interpret as silicate power of density 0.5 ± 0.5 g cm^{-3}. Recently, R. Clancy, A. Grossman, and D. Muhleman mapped Mars in emission at 1.3 cm with the VLA. The Stealth region clearly stood out as material with near unity emissivity; these data confirm the nearly zero reflectivities. The photogeology of the units contained in Stealth has been discussed by P. H. Schultz and A. B. Lutz, *Icarus* **73**, 91 (1988); A. W. Ward, *J. Geophys. Res.* **84**, 8147 (1979); J. A. Cutts and R. S. U. Scott, *ibid.* **78**, 4139 (1973).
18. L. Gaddis *et al.*, *Geol. Soc. Am. Bull.* **101**, 317 (1989).
19. Thermal inertia values for Mars are obtained by comparing the diurnal thermal IR emission to a thermal model. The resulting values depend on bulk soil density through the thermal conductivity to depths of ≈1 cm or several centimeters. The altitude of a given deposit may affect the inertia because of the thermal conductivity of the martian atmosphere. The standard data set is in F. D. Palluconi and H. H. Kieffer [*Icarus* **45**, 415 (1981)]; see also P. Christensen, *ibid.* **68**, 217 (1986).
20. A homogeneous sublayer with a dielectric constant of 3 was used in the calculations, but the results are nearly independent of this value.
21. S. W. Lee, P. C. Thomas, and J. Veverka [*J. Geophys. Res.* **87**, 10025 (1982)] have shown that wind streaks on the west flank of Arsia Mons indicate that the surface winds flowed downslope, from east to west, into our Stealth region. See also, P. Thomas and J. Veverka, *J. Geophys. Res.* **84**, 8131 (1979); P. H. Schultz and A. B. Lutz, in (*17*).
22. D. H. Scott and K. L. Tanaka, *Icarus* **45**, 304 (1981); *U.S. Geol. Surv. Misc. Geol. Invest. Map I-1802-A* (1986).

23. We thank the observing staffs at the VLA and the 70-m facilities for their attention and care in performing the observations; D. Paige and B. Jakosky for discussions about martian geology; and several members of the VLA professional staff including K. Sowinsky and T. Cornwell concerning the endlessly complex data processing; and J. Head, L. Keszthelyi, A. Ingersoll, H. Kieffer, S. Murchie, and R. Simpson for comments concerning the manuscript. Supported under NASA grant NAGW 1499 and National Science Foundation grant AST89-19698, and the state of Maryland through the Laboratory for Millimeter Wave Astronomy (A.G.). JPL is operated by the California Institute of Technology under a contract NASA. Contribution number 4993 from the Division of Geological and Planetary Sciences, California Institute of Technology.

14 May 1991; accepted 12 August 1991